IEEE Access
Multidisciplinary | Rapid Review | Open Access Journal

Received February 10, 2021, accepted March 1, 2021, date of publication March 8, 2021, date of current version March 15, 2021.

Digital Object Identifier 10.1109/ACCESS.2021.3064058

Experimental Research on Over-Range Measurement Method Based on Quasi-Digital Direct-Current Leakage Current Sensor

NINGZHAO LUO, FENG YANG, YAO ZHANG, AND SHAOLI LI
College of Electrical Engineering, PLA Naval University of Engineering, Wuhan 430033, China
Corresponding author: Shaoli Li (past97molly@outlook.com)

ABSTRACT As for the direct-current (DC) power systems, the DC leakage current sensor is indispensable for positioning insulation faults. And in this paper, a quasi-digital flux gate sensor was designed based on duty ratio model, and the mathematical model between the excitation voltage period and the measured current which exceeded the measurement range was built by analyzing the working principles of the duty-ratio model digital sensor. In this way, the measurement range of the original sensor could be expanded to 1.5 times of its original. Meanwhile, without changing the hardware, the solution provided in this paper also solved the measurement failure problem of part of sensors when the any overcurrent situations happen in the system, such as overload or short-circuit. Besides, the sensor designed in this paper could achieve Level-0.1 measurement accuracy within range, and reach Level-2 over-range measurement accuracy, satisfying the demands of DC power supply system on leakage current measurement.

INDEX TERMS Current sensor, over-range, flux gate.

I. INTRODUCTION

The DC system has become the tendency of power system development. The direct current has been taken as the main power distribution form in fields of electric vehicles, ships, microgrids, and new energy sources [1]–[4]. In order to guarantee the reliability of the DC system operating, and improve the power supply continuity of the load, it is usually necessary to configure the DC insulation monitoring device to troubleshoot the system insulation fault [5]–[7]. As a matter of fact, the insulation fault positioning of the DC system depends on the DC leakage current sensor. The sensor having higher accuracy and larger measurement range can achieve larger range measurement of the insulation fault and reflect more accurate trend of the system insulation degradation [6], [7]. In recent years, various types of high-accuracy and high-bandwidth DC current sensors have been designed in a couple of papers to meet the ever growing demands on measurement [8]–[10], among which, the flux gate sensor was designed to measure the DC leakage current of the system [11]–[13]. In 2009, a research team led by Xu Zeliang of Siemens (China) Co., Ltd. designed a B-type residual current detector based on self-excited oscillation applying magnetic modulation principle. This detector is featured in closed-structure of magnetic core with an inner diameter of 43mm, DC current measurement range of ± 2A, and DC linearity error of 10% [11]. In 2015, Wang Yao *et al.* from Hebei University of Technology proposed a magnetic modulation AC/DC leakage current detection method based on all-phase Fourier transform, which on one hand, simplifies the structure of the transformer while on the other hand, optimizes the structure of the demodulation circuit. Its designed magnetic core is of a closed structure with less than 20mm inner diameter, ±2.2A DC current measurement range, and less than 5% detection error rate [14]. In 2016, the research team led by Yang Xiaoguang of Hebei University of Technology optimized and upgraded the previously proposed current sensor solution which was based on two-magnetic-core three-winding. The new version expanded the range from the original ±20A to ±25A, and enhanced the measurement accuracy at full scale from original 0.7% to 0.4% [15], [16].

As for the DC power system, the electromagnetic environment to deploy the leakage current sensor is usually quite complex, containing rectifier or inverter which can interfere the work of sensors. In 2015, Academician Zhang Zhonghua

The associate editor coordinating the review of this manuscript and approving it for publication was Wei Xu.

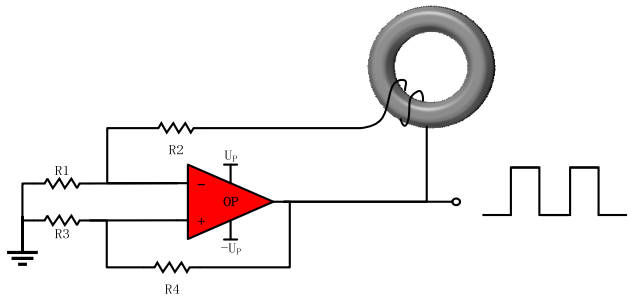

FIGURE 1. Circuit diagram of leakage current sensor.

proposed [17] the duty ratio model sensor for measuring large DC current. According to the principles of the such sensors based on duty-ratio model, and combining with specific design for the sensor core, excitation coil and external circuit, it was made to be able to measure small leakage current in this paper, which is convenient for insulation measurement. Meanwhile, the situation that the measured current exceeds the sensor range was also analyzed to establish relative models and conduct empirical study. The results show that, under the precondition of no hardware change, the duty ratio model sensor could improve the measurement range of the sensor by measuring excitation voltage period. This provides a solution for using this type of sensors to carry out over-range measurement, such as overload and short-circuit current, etc.

II. DUTY RATIO MODEL SENSOR OPERATING PRINCIPLE

The leakage current of the DC system is I, the excitation coil is wound on the iron core with windings of W_1. The R_1, R_2, R_3 and R_4, as well as the operational amplifier and the excitation coil constitute a self-excited oscillation circuit. The operational amplifier acts as a comparing unit. And the impedance of the excitation coil is equivalent to the resistance R_2. According to the working principles of flux gate technology, when the circuit encounters self-excited oscillation, the operational amplifier outputs the square wave of a certain frequency. The amplitude of the positive and negative half cycles of the square wave should be equal to the power supply voltage $\pm U_P$ of the operational amplifier. The operational amplifier drives the excitation coil to make the iron core be in the over-saturated state of alternated positive and negative magnetic flux. When the measured cable contains leakage current, the current I would generate bias magnetic flux in the iron core, which is opposite to the magnetic flux generated by operational amplifier when it outputs positive voltage; and is of the same phase with that of the magnetic flux generated by operational amplifier when it outputs negative voltage. This result in gradual increase of iron core magnetic flux along clockwise direction. When $I_1 = -I_S$, the iron core is saturated, the excitation coil inductance changes from L_1 of the unsaturated state to L_0 after being saturated, showing decreased inductance, reduced circuit time constant, and increased current change rate; If $I_1 = I_T$ and reaching reversal current, the voltage across both ends of the resistor R_1 is equal to the voltage at the in-phase input end, and the

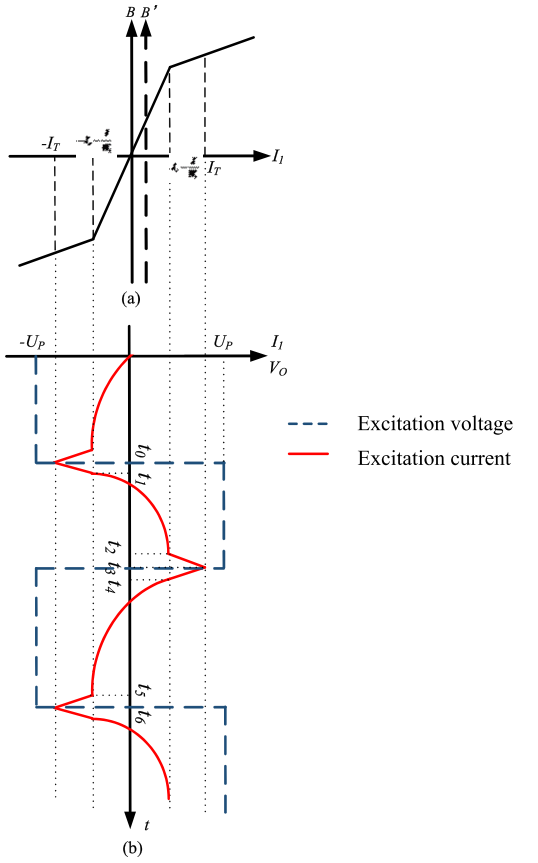

FIGURE 2. Magnetization curve/waveforms of excitation voltage and current.

operational amplifier outputs flips, $V_O = U_P$.

$$I_T = \frac{R_3}{R_1(R_3 + R_4)} U_P \tag{1}$$

Then being driven by forward voltage V_O, the amplitude of the excitation current I_1 keeps decreasing. When $I_1 = -I_S$, the excitation coil belongs no longer saturated, and has increasing magnetic reluctance, and the inductance changes from L_0 to L_1. When I_1 rises to $I_1 = I_S$, the sensor core becomes saturated again. When $I_1 = I_T$, the output of the operational amplifier flips and $V_O = -U_P$. The above process repeats time and time again. The operational amplifier outputs a periodic square wave, and the excitation coil forms a self-oscillation.

The output voltage of the operational amplifier and the current waveform in the excitation coil are as shown in Figure 2. Suppose that the leakage current $I = 0$A, due to the symmetry of the core magnetization curve, all parameters of the self-excited oscillation circuit are in a symmetrical state, and the average values of the excitation voltage and excitation current in one cycle are both zero. If the cable has any leakage current which generates the counterclockwise magnetic flux in the iron core, the excitation current required for the iron core to reach positive saturation is reduced to $I_S - I/W_1$, and the excitation current required to reach the negative saturation turns to be $-I_S - I/W_1$. The magnetization curve of the

iron core is as shown in Figure 2(a). It is equivalent to the rightward shifting of the coordinate system. According to the core magnetization curve and the measured current, the sensor can work in three modes [18]–[20]:

Case 1: if the measured current is small, the excitation square wave voltage can make the iron core saturated no matter in the positive-half cycle or negative-half cycle, namely:

$$I_T - \frac{|I|}{W_1} > I_S \tag{2}$$

Case 2: if the measured current gets greater, the iron core is in saturation state when the excitation square wave voltage is in the positive half cycle, but cannot get saturated in the negative half cycle; or the core gets saturated when the excitation square wave is in the negative half cycle, but cannot enter saturation state in the positive half cycle, namely:

$$\begin{cases} I_T + \dfrac{|I|}{W_1} > I_S \\ I_T - \dfrac{|I|}{W_1} < I_S \end{cases} \tag{3}$$

Case 3: if the measured current is too large, the excitation square wave voltage cannot get the iron core out of saturation state, and the excitation coil inductance is always L_0. That is

$$\frac{|I|}{W_1} - I_T > I_S \tag{4}$$

In order to analyze the working process of the sensor, it is assumed that the magnetization curve is a piecewise linear curve, the iron core has no coercive force, the excitation coil inductance is L_0 when the core is in saturation state, the excitation coil inductance is L_1 when the core is not saturated, and $L_0 \ll L_1$. The voltage and current equations of the circuit under saturated and unsaturated conditions respectively are as below:

$$V_O = \begin{cases} (R_1 + R_2)i_1(t) + L_0 \dfrac{di_1(t)}{dt} \\ (R_1 + R_2)i_1(t) + L_1 \dfrac{di_1(t)}{dt} \end{cases} \tag{5}$$

If the output voltage of the operational amplifier does not flip, the maximum steady-state current of the loop formed by the resistors R_1, R_2 and the excitation coil is:

$$I_M = \frac{U_P}{R_1 + R_2} \tag{6}$$

The expression of the excitation current changes with time in Case 1, and the expression of excitation voltage duty-ratio could be given out and calculated easily according to the circuit calculation rules. Relevant calculation methods have been given out in Literature [18]:

$$D = \frac{T_P}{T_1} = \frac{t_3 - t_0}{t_6 - t_0} \approx \frac{1}{2} - \frac{1}{2W_1(I_M - I_S)} I \tag{7}$$

It can be seen from Formula (7) that the waveform duty ratio of the square wave excitation voltage approximately maintains linear relations with the measured leakage current. When the leakage current is $I = 0$A, the duty ratio D = 50%.

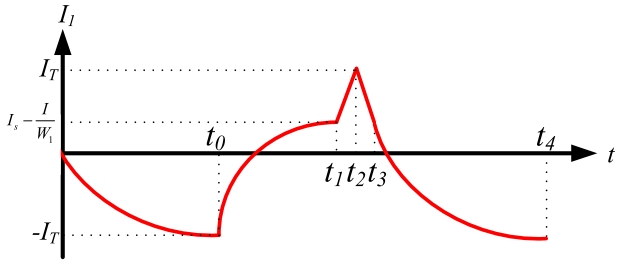

FIGURE 3. Situation2: waveforms of excitation current.

That's the principle of duty-ratio model sensor. Therefore, the value of the leakage current can be calculated by taking MCU to measure the duty-ratio of excitation voltage. And the purposes of sensor digitalization and non-interference of circuit measuring could be thereby achieved without ADC. So, it is suitable for being used in places with intensively deployed electronic devices, like ships.

III. PRINCIPLE OF OVER RANGE MEASUREMENT

If the measured current continues to increase, the iron core gets saturated when the excitation square wave voltage is in the positive half cycle, but cannot enter saturation state during the negative half cycle. The current waveform flowing through the resistor R_1 is as shown in Figure 3.

The time and current equations of Case 2 are as below:

$$i_1(t) = \begin{cases} I_M + (-I_T - I_M)e^{\frac{t_0 - t}{\tau_1}} & t_0 < t < t_1 \\ I_M - (I_M - I_S + \dfrac{I}{W_1})e^{\frac{t_1 - t}{\tau_0}} & t_1 < t < t_2 \\ -I_M + (I_T + I_M)e^{\frac{t_2 - t}{\tau_0}} & t_2 < t < t_3 \\ -I_M + (I_M + I_S - \dfrac{I}{W_1})e^{\frac{t_3 - t}{\tau_1}} & t_3 < t < t_4 \end{cases} \tag{8}$$

It can be solved by calculating the time intervals of t_0, t_0, t_2, t_3, and t_4 that:

$$\begin{cases} t_1 - t_0 = \tau_1 \ln\left(\dfrac{I_M + I_T}{I_M - I_S + \frac{I}{W_1}}\right) \\ t_2 - t_1 = \tau_0 \ln\left(\dfrac{I_M - I_S + \frac{I}{W_1}}{I_M - I_T}\right) \\ t_3 - t_2 = \tau_0 \ln\left(\dfrac{I_M + I_T}{I_M + I_S - \frac{I}{W_1}}\right) \\ t_4 - t_3 = \tau_1 \ln\left(\dfrac{I_M + I_S - \frac{I}{W_1}}{I_M - I_T}\right) \end{cases} \tag{9}$$

$\tau_0 \ll \tau_1$, the oscillation period can be calculated as below:

$$T_2 \approx \tau_1 \ln\left(\frac{I_M + I_T}{I_M - I_S + \frac{I}{W_1}}\right) + \tau_1 \ln\left(\frac{I_M + I_S - \frac{I}{W_1}}{I_M - I_T}\right) \tag{10}$$

Since $I_M \gg I_S$, $I_M \gg I/W_1$, the square wave oscillation period T_2 of Case 2 could be simplified as below:

$$T_2 \approx 2\tau_1 \frac{I_T + I_S}{I_M} - \frac{2\tau_1}{I_M W_1} I \tag{11}$$

It can be known from Formula (11) that, when the measured current exceeds the measurement range of the duty ratio model sensor, the period of the self-oscillated square wave decreases with the measured current increase.

If the measured current continues to increase, it can result in over-large current and enter situation described in Case 3. Supposing that the magnetization curve is a piecewise linear function [21], the period of the self-oscillated square wave will remain unchanged with the increase of the measured current. But in fact, the magnetic permeability of the iron core will change with the increase of the measured current, showing changes characterized in arc tangent function properties. That is, approaching to a setting value gradually. In Case 3, the period of the self-excited oscillation square wave will keep decreasing with the increase of the measured current. However, since the degree of decrease reduces, the period change seems not so significant. In summary, once the measured current exceeds the range of the duty ratio model sensor, the period of self-excited oscillation will continue to decrease. That is: when the current exceeds the range, the size of the measured current can be determined by measuring the square wave period. As a matter of fact, the measurement of square wave period is the precondition for measuring duty ratio. Therefore, the duty ratio model sensor can achieve over-range measurement without any changes in hardware. Theoretically, the measurement range of the duty ratio model sensor can be extended easily.

According to Equations (10) and (11), the sensitivity of the sensor in cases 1 and 2 can be calculated as:

$$S_1 = \frac{d(DT_1)}{dI} = \frac{2I_S\tau_1}{W_1 I_M(I_M - I_S)} \tag{12}$$

$$S_2 = \frac{d(T_2)}{dI} = \frac{2\tau_1}{W_1 I_M} \tag{13}$$

$I_M \gg I_S$, By comparing the values of S_2 *and* S_1, we can get:

$$\frac{S_2}{S_1} = \frac{\mathrm{I_M}}{\mathrm{I_S}} - 1 \gg 1 \tag{14}$$

In case 2, the time for the iron core to enter the unsaturated state is prolonged, and the average inductance of the coil is rapidly reduced, resulting in a rapid decrease in the oscillation period. At this time, the sensor sensitivity is greatly improved, which is convenient for the detection of small current.

IV. SENSOR PARAMETER

The leakage current sensor is mainly composed of iron core, coil, self-excited oscillation circuit, shielding layer and measurement circuit.

It can be known from the working principle of the sensor that, the iron core works in a periodic saturation state. In order to achieve accurate measurement, the iron core usually needs to satisfy the following requirements:

(1) High magnetic permeability: the higher the magnetic permeability of the core in the unsaturated state, the greater the change of magnetic permeability in saturated state, and the greater the effective signal provided by the sensor. This can help to improve the sensor sensitivity. But the sensor with high magnetic permeability is usually more sensitive which could result in larger noise sound.

(2) Low coercive force: the magnetic field generated by small leakage current is relatively weaker, which could achieve higher resolution for measurement of small current, thus to reduce the overall power consumption of the sensor.

(3) Low saturation magnetization makes iron core get saturated easier, and achieves higher sensitivity of sensor.

(4) The difference between the outer diameter and the inner diameter of the iron core is small. The principle of the flux gate sensor requires that the iron core enters the saturation state while being excited. If the difference between the inner and outer diameters of the iron core is too large, the magnetic flux is likely to be uneven, which could result in measurement errors.

Moreover, the iron core should also have comparatively high resistivity, low electromagnetic noise, and low magnetostriction. All these characteristics can effectively reduce the power consumption and improve the signal-to-noise ratio of the sensor.

TABLE 1. The parameters of soft magnetic material.

Materials	B_S T	H_c $A{\cdot}m^{-1}$	μ_r	λ_S 10^{-6}	P $\mu\Omega{\cdot}cm$
6.5% silicon steel	1.89	40	100	82	68
Permalloy 1J86	0.75	0.64	150000	-0.6	55
Cobalt-based amorphous 2714A	0.57	0.2	170000	1	142
Fe-based nanocrystalline FeCuNbSiB	1.24	0.53	157000	2.1	120

A. MATERIAL SELECTION

It can be seen from the requirements that, materials that satisfy the above conditions are usually soft magnetic materials. Therefore, the iron core of the flux gate sensor is usually made of permalloy, amorphous materials, or nanocrystalline materials.

It can be seen from Table 1 that the hysteresis and permeability of silicon steel sheets are slightly lower, which is not suitable. Permalloy, cobalt-based amorphous and Fe-based nanocrystals are all suitable for being used to make sensor cores. Among the above, the permalloy and cobalt-based amorphous materials are of better parameters. But amorphous materials are usually brittle and fragile, not suitable for being used in places with shock and vibration, such as ships. There have been cases where amorphous material transformers have failed the impact test. Therefore, as for sensors used on ships, the Permalloy materials should be the best choice. Then, the iron core saturation can be calculated according to the ampere loop theorem:

$$I = Hl = \frac{Bl}{\mu} \tag{15}$$

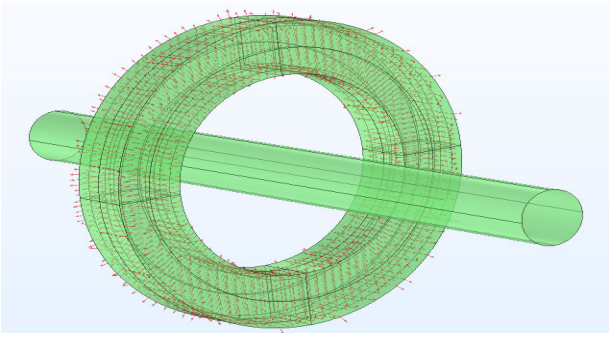

FIGURE 4. Flux gate simulation model.

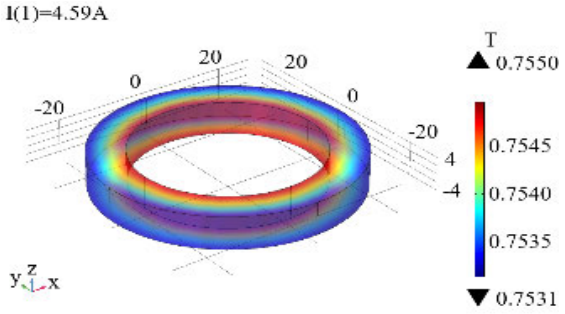

Positive Excitation Flux

FIGURE 5. COMSOL simulation of magnetic flux density.

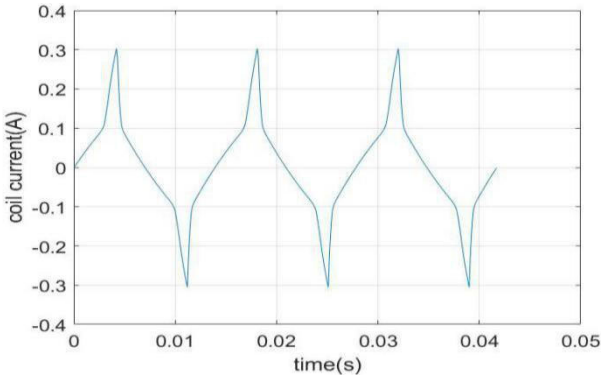

FIGURE 6. Waveform of coil current change under normal conditions.

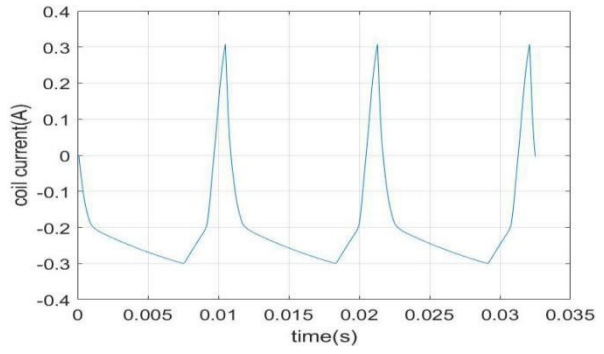

FIGURE 7. Coil current change waveform when over-range.

The inner diameter of the sensor core is D = 40mm. Supposing that the difference between the inner and outer diameters of the core is much smaller than the inner diameter, l is the equivalent magnetic path length of the core $l \approx \pi D =$ 126mm, it can be calculated by Formula (15) that, when the leakage current is 1A, the magnetic field strength B inside the iron core is about 1.7T∼2.5T.

For the iron core with an inner diameter of $\Phi = 40$mm, if enameled wire with an outer diameter of $\Phi_q = 0.35$mm is used for winding, the number of winding turns required to cover the entire iron core should be:

$$W_1 \geq \frac{\pi \Phi}{\Phi_q} = 359 \tag{16}$$

The resistance of the 359 winding turns of excitation coil $R_2 = 2.26\Omega$ can be calculated according to the resistivity of the enameled wire.

The resistance of R_3 and R_4 have little effect on the measurement result and plays the role of calibrating the reverse voltage. The values of R_3 and R_4 should not be too large, and should match the input impedance of the operational amplifier. Changing the R_3 and R_4 ratio can change the square wave frequency of the excitation voltage. The lower the ratio, the higher the frequency. Usually R_3 and R_4 should be less than 100kΩ. In order to ensure that the excitation current can make the iron core get in deep saturation, $R_1 = 1$kΩ.

Simultaneously, the flux gate sensor is simulated in COMSOL. As shown in Figure 4, the coil is wound on the toroidal core. The red arrow is the direction of the coil current, and the measured current flows through the core. Among them, the number of turns of the coil is 1000, the cross-sectional area of the coil wire is 10^{-7}mm^2, and the conductivity is 6×10^7S/m. Among them, the core inner diameter $r = 40$mm, outer diameter $R = 56$mm, and relative permeability $\mu_r = 150000$.

Through COMSOL simulation, the internal magnetic field strength of the iron core is as shown in Figure 5. The iron core can reach deep saturation in forward excitation.

When the measured current flowing in the middle of the iron core I = 0A, after applying a square wave voltage to the iron core coil, the current change of a section of the coil is intercepted as shown in Figure 6.

It can be seen from the figure that the current oscillation period T of the iron core coil under normal working conditions is about 0.014s, the frequency f = 71.4Hz, and the coil current is 0.1A, the iron core enters a saturated state. At this time, the coil inductance changes and the current change rate change. The duty cycle of the square wave voltage is 50%.

Then continuously increase the measured current value in the middle of the magnetic core, and at the same time apply a square wave voltage to the magnetic core coil, and intercept a section of the coil current change as shown in Figure 7:

It can be seen from the figure that the current oscillation period of the magnetic core coil is about 0.011s, the frequency, the coil applies a reverse excitation square wave

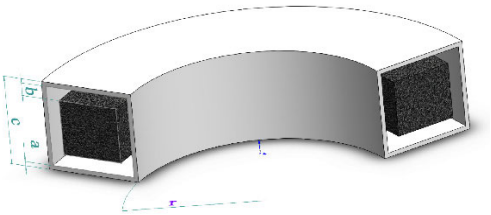

FIGURE 8. Structure diagram of shielding layer.

voltage until the current value reaches the reverse current, the magnetic core still cannot enter the saturation state.

B. SHIELDING DESIGN

The external magnetic field can significantly affect the measurement results of the flux gate sensor, so a shielding structure needs to be fitted on the flux gate sensor. The shielding structure is an outer shell of sensor, which is made of high permeability material. It is mainly used to shunt the external interference magnetic field, thereby guiding most of the low-frequency interference magnetic fields to pass through the shell instead of passing through iron core, thus to reduce the disturbance to the measurement. The shielding structure is as shown in Figure 8.

The shielding structure is featured in thickness of a, interval of b between the iron core and itself, external width of c, relative permeability of μ_r, external interference magnetic flux of Φ_0, and the magnetic flux Φ_1 flowing through the shield, as well as a small part of the magnetic flux Φ_2 penetrating from the shield to the inside.

$$\Phi_0 = \Phi_1 + \Phi_2 \tag{17}$$

The formula of the magnetic shielding effectiveness S can be obtained by calculating the magnetic circuit of the shielding layer [22]:

$$S = \frac{\Phi_0}{\Phi_2} = \frac{12}{(r + c/2)^2 \pi^2} \times \mu_r \times \frac{ab(c-a)}{c-b-2a} + 1 \tag{18}$$

In order to ensure the shielding effect, the 1.5mm thick 1J86 permalloy which is made of the same material as that of the iron core is applied. $\mu_r = 150000$, $a = 1.5mm$, $b = 12.5mm$, $c = 36mm$, and inner diameter $r = 30mm$. The shielding effectiveness can be calculated according to Formula (18):

$$S = 25004 \tag{19}$$

This means that, the external magnetic flux interference can be weakened to 0.00004 time of the original. Except encountering an extremely strong pulse magnetic field, the general magnetic field interference can be well shielded, satisfying the design requirements.

V. EXPERIMWNTAL VERIFICATION

The platform takes Keithley 2461 source meter as the measured current reference, which can maximumly outputs 10A current with 0.02% current precision. The actual current,

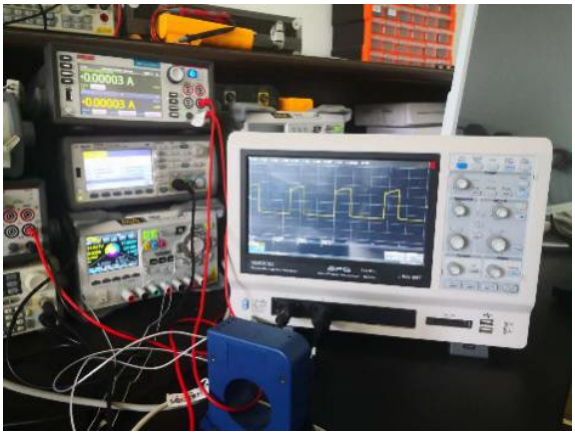

FIGURE 9. Testing platform.

which is measured by the calibrated Keithey DMM7510 7-and-a-half digits multimeter can be taken as the standard current. NPLC = 10 to satisfy sufficient precision. The duty ration measurement is achieved by all Agilent experiments in lab conditions. The ambient temperature is set as 25 °C. Since the sensor is installed inside the emergency switchboard of the ship, and the cabin has been equipped with air conditioner to adjust the temperature which guarantees small temperature change, the sensor has little requirement on temperature drift, so the experiment excludes examination on the temperature drift.

In the experiment, the testing range of the measured current reference is 0-1A. The measurement is carried out once every 5mA within 0-100mA range, and once every 20mA within 200mA-1A range.

As for the experimental results of the duty ratio model sensor, please refer to Figure 10. The measurement range of this sensor is ±1A, and the range of the duty ratio output is about 10-90%. The reverse current test result is consistent with that of the forward current. Therefore, only the parameters of the forward current experiment are given. It can be seen from the experimental results that within the 0-1A measurement range, the output duty ration of the sensor is basically linear. When the measured current exceeds 800mA and approaching range limits, the sensor is close to the saturation region and is affected by the nonlinear magnetization curve of the iron core. At this time, the test data error is large. But within the 0-1A range, the absolute error of the sensor duty ratio output is less than 0.01A. And at this time, the sensor accuracy is higher than Level-1, which has already met the application requirements of the sensor.

The leakage current required to be measured is usually within 500mA. Therefore, the sensor's measurement precision within 0-500mA testing range is examined. The results show that, the absolute error of the duty ratio output at that time is less than 0.0004, and the sensor accuracy is higher than Level-0.05. Meanwhile, the designed range of the duty ratio model sensor should be 200% of the actually required range, thereby preventing too large measurement error caused by iron core linearity, and improving measurement accuracy.

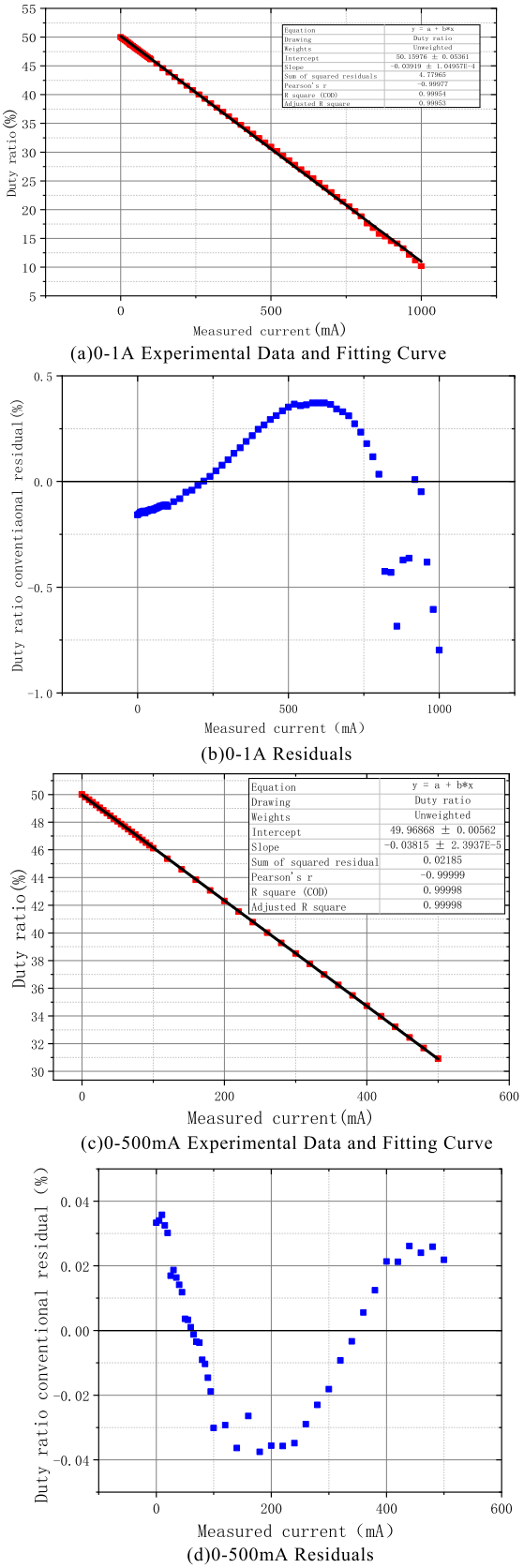

FIGURE 10. The duty ratio model experimental data and fitting curve.

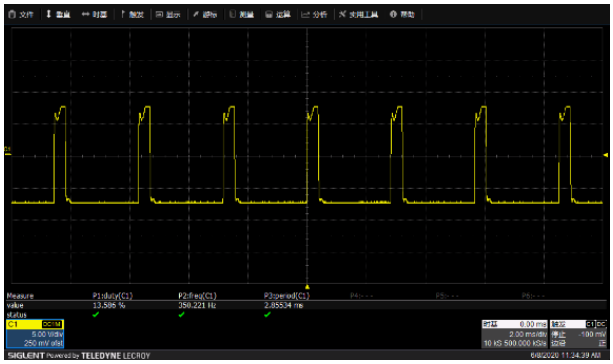

FIGURE 11. The duty ratio model experimental ware.

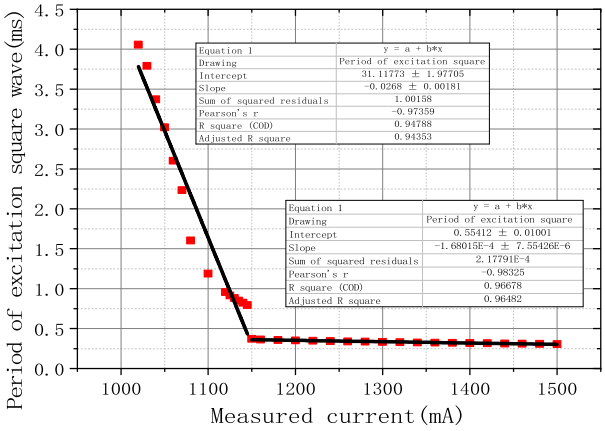

FIGURE 12. The duty ratio model experimental data and fitting curve.

When the measured current exceeds the measurement range of the sensor, the duty ratio of the square wave excitation voltage is further measured, from which, it is figured out that the duty ratio changes in reverse and the rate of change gradually decreases, failing to reflect the change of the measured current. But at this time, the period of the square wave excitation voltage continuously decreases. As for the excitation voltage waveform, please see Figure 11.

The excitation voltage period decreases monotonously with the increase of the measured current. The measurement results are as shown in Figure 12, containing two obvious quasi-linear areas. This is corresponding to Case 2 and Case 3 as mentioned above. Linear fitting could be conducted to the two cases, thus to obtain the calculation formula of the measured current.

Due to the saturation and nonlinearity of the iron core, the relative error in Case 2 is comparatively large. The maximum error reaches 20mA, and the sensor accuracy is within Level-2. This can basically satisfy the measurement demand of leakage current, and the relative error can be less than 1%. After entering Case 3, the iron core gets fully saturated, and the resolution is reduced, so that the sensor accuracy is at about Level-2.

Table 2 shows the standard deviation and peak-to-peak value of the duty ratio and square wave period of the

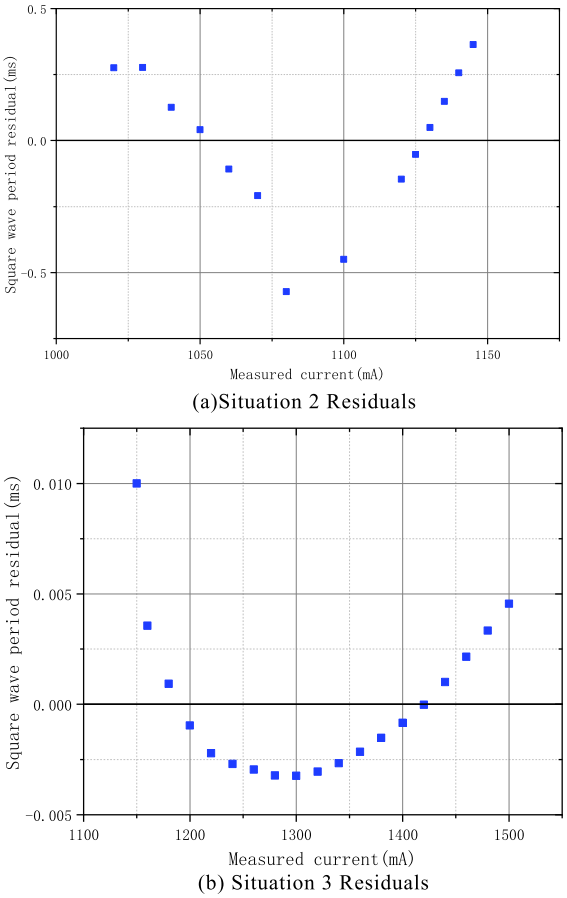

FIGURE 13. Over range fit residuals.

TABLE 2. The P-P and StdDev parameters of duty ratio and period.

Current (mA)	StdDev of duty ratio (mPct)	P-P of duty ratio (mPct)	StdDev of Period (ns)	P-P of Period (ns)
0	10.10	54.63	333.7	2428
200	12.69	76.42	650.3	4413
400	10.15	56.70	399.5	2573
600	11.10	71.82	1030.4	4566
800	79.58	765.8	1729.1	8991
1000	1542.2	2991.0	123631	632509
1050	59.67	375.75	7.64	47.40
1200	29.27	194.24	16.45	108.58
1400	24.42	207.09	10.75	45.45

waveform that is output by the sensor under different measured currents, from which, it can be seen that the output duty ratio and square wave period are the most unstable when the sensor measures at 1A. Then after exceeding the measuring range, it enters the sensor saturation area, where the output period value has little fluctuation, and shows stable measurement results. Therefore, it should avoid using this type of sensor at full range situation.

The sensitivity of the sensor can be obtained through calculation. In case 1, the sensitivity is about 1.36ms/A, while in case 2, the sensitivity can be up to 27.7ms/A, which is 20 times higher than that in case 1.

VI. CONCLUSION

In this paper, a DC leakage current sensor is designed by the flux gate scheme based on duty ratio model. It is featured in high measurement accuracy and good stability. Since it adopts digitalized design, it can hardly be affected by external electromagnetic interference, and suitable for being used in places with complicated electromagnetic environment, such as ships.

If the measured current exceeds the design range of the sensor, the over-range current can be measured by measuring the excitation voltage period. As a matter of fact, this solution helps to enlarge sensor range which is 1.5 times of the original, but still maintains Level-2 accuracy. If adopting high-order polynomial fitting method, the over-range accuracy of the sensor can be further improved.

It is also figured out from the experiment that in the over-range region, the period of the sensor excitation voltage is extremely sensitive to the measured current. At this time, the sensor sensitivity is higher than that within the range. The change of the 100mA measured current causes 3ms change of excitation voltage period and the sensitivity is increased by 20 times. This feature can be applied to measure the micro current fluctuations of large current load. And its characteristics need to be further studied.

REFERENCES

[1] X. Gao and L. Fu, "SOC optimization based energy management strategy for hybrid energy storage system in vessel integrated power system," *IEEE Access*, vol. 8, pp. 54611–54619, 2020.

[2] S.-K. Lim, H.-S. Lee, H.-R. Cha, and S.-J. Park, "Multi-level DC/DC converter for e-mobility charging stations," *IEEE Access*, vol. 8, pp. 48774–48783, 2020.

[3] M. Tabari and A. Yazdani, "Stability of a DC distribution system for power system integration of plug-in hybrid electric vehicles," *IEEE Trans. Smart Grid*, vol. 5, no. 5, pp. 2564–2573, Sep. 2014.

[4] R. Li and F. Shi, "Control and optimization of residential photovoltaic power generation system with high efficiency isolated bidirectional DC–DC converter," *IEEE Access*, vol. 7, pp. 116107–116122, 2019.

[5] G. Qiao, "Research on application of insulation monitoring technology for DC system of power plant," M.S. thesis, Dept. Electron., North China Electr. Power Univ., Beijing, China, Tech. Rep., 2018.

[6] Q. Song, "Principle research and hardware design of insulation monitoring system for ship power station," *Ship Sci. Technol.*, vol. 40, no. 4, pp. 70–72, Feb. 2018.

[7] L. Qi and Z. Ye, "A design of feeble current transformer for insulation monitoring of naval vessel power network," *J. Nav. Univ. Eng.*, vol. 13, no. 2, pp. 79–86, Apr. 2001.

[8] P. Ripka, K. Draxler, and R. Styblikova, "Measurement of DC currents in the power grid by current transformer," *IEEE Trans. Magn.*, vol. 49, no. 1, pp. 73–76, Jan. 2013.

[9] B. Dufay, S. Saez, C. Dolabdjian, A. Yelon, and D. Menard, "Development of a high sensitivity giant magneto-impedance magnetometer: Comparison with a commercial flux-gate," *IEEE Trans. Magn.*, vol. 49, no. 1, pp. 85–88, Jan. 2013.

[10] X. Yang, Y. Li, W. Guo, W. Zheng, C. Xie, and H. Yu, "A new compact fluxgate current sensor for AC and DC application," *IEEE Trans. Magn.*, vol. 50, no. 11, Nov. 2014, Art. no. 4005704.

[11] X. Zeliang, M. Yingzong, D. Feng, Z. Yue, and M. Anheuser, "Type B RCD with a simplified magnetic modulation/demodulation method," in *Proc. IEEE 6th IPEMC*, Wuhan, China, May 2009, pp. 769–772.

[12] M. Yingzong, D. Feng, C. Weigang, Z. Yue, and M. Anheuser, "An AC/DC sensing method based on adaptive magnetic modulation technology with double feedback properties," in *Proc. IEEE Int. Workshop AMPS*, Sep. 2011, pp. 48–52.
[13] C.-F. Cheng, R.-S. Li, and J.-R. Chen, "Design of the DC leakage current sensor with magnetic modulation-based scheme," in *Proc. IEEE ISIE*, May 2013, pp. 1–6.
[14] W. Yao, L. Kui, R. Bofei, Z. Xu, and G. Leijiao, "Study of fluxgate current detecting method for AC-DC Earth leakage current based on apFFT," *Trans. China Electrotech. Soc.*, vol. 30, no. 18, pp. 254–260, Sep. 2015.
[15] X. Yang, W. Guo, C. Li, B. Zhu, T. Chen, and W. Ge, "Design optimization of a fluxgate current sensor with low interference," *IEEE Trans. Appl. Supercond.*, vol. 26, no. 4, pp. 1–5, Jun. 2016.
[16] X. Yang, W. Guo, C. Li, B. Zhu, L. Pang, and Y. Wang, "A fluxgate current sensor with a U-shaped magnetic gathering shell," *IEEE Trans. Magn.*, vol. 51, no. 11, pp. 1–4, Nov. 2015.
[17] Z. Zhang *et al.*, "The utility model relates to a single magnetic core quasi-digital DC large current sensor," CN Patent 2015 100 117 746, Oct. 8, 2015.
[18] P. Pejovic, "A simple circuit for direct current measurement using a transformer," *IEEE Trans. Circuits Syst. I, Fundam. Theory Appl.*, vol. 45, no. 8, pp. 830–837, Aug. 1998.
[19] I. M. Filanovsky and L. Taylor, "Circuit with nonlinear transformer allowing DC current measurements via an isolation gap," in *Proc. 35th Midwest Symp. Circuits Syst.*, 1992, pp. 318–323.
[20] K. Li, F. Niu, Y. Wu, Y. Wang, Y. Dai, L. Wang, and E. Li, "Nonlinear current detection based on magnetic modulation technology," *IEEE Trans. Magn.*, vol. 51, no. 11, pp. 1–4, Nov. 2015.
[21] N. Wang, Z. Zhang, Z. Li, Y. Zhang, Q. He, B. Han, and Y. Lu, "Self-oscillating fluxgate-based quasi-digital sensor for DC high-current measurement," *IEEE Trans. Instrum. Meas.*, vol. 64, no. 12, pp. 3555–3563, Dec. 2015.
[22] X. Wang, "Study on magnetic shielding effectiveness of heavy direct current sensor," Ph.D. dissertation, Dept. Electron., Huazhong Univ. Sci. Technol., Hubei, China, Tech. Rep., 2007.

NINGZHAO LUO received the Ph.D. degree in electrical engineering from the PLA Naval University of Engineering, Wuhan, China, in 2012. From 2013 to 2016, he was a Postdoctoral Research Scholar in control engineering with the PLA Naval University of Engineering. Since 2014, he has been with the College of Electrical Engineering, PLA Naval University of Engineering, where he is currently an Associate Researcher. His current research interests include safe operating of marine power systems and power system monitoring.

FENG YANG received the Ph.D. degree in electrical engineering from the PLA Naval University of Engineering, Wuhan, China, in 2011. He is currently a Professor with the PLA Naval University of Engineering. His current research interest includes power system monitoring and protection.

YAO ZHANG received the B.E. degree in electrical engineering from Harbin Engineering University, Harbin, China, in 2018. He is currently pursuing the M.E. degree with the College of Electrical Engineering, PLA Naval University of Engineering, Wuhan, China. His research interests include pulsed eddy current testing, dc leakage current detection, and power system protection.

SHAOLI LI received the B.E. degree in electrical engineering from North China Electric Power University, Baoding, China, in 2019. He is currently pursuing the M.E. degree with the College of Electrical Engineering, PLA Naval University of Engineering, Wuhan, China. His research interests include pulsed eddy current testing, electromagnetic acoustic transducer, and pipeline corrosion detection technology.